Version of Record: https://www.sciencedirect.com/science/article/pii/S0927650522000172
Manuscript_dbe62b5fd35ae38c07f05eceee9d4f32

A study of events with photoelectric emission in the DarkSide-50 liquid argon Time Projection Chamber

P. Agnes[a], I. F. M. Albuquerque[b], T. Alexander[c], A. K. Alton[d], M. Ave[b], H. O. Back[c], G. Batignani[h,i], K. Biery[al], V. Bocci[x], W. M. Bonivento[j], B. Bottino[k,l], S. Bussino[m,n], M. Cadeddu[j], M. Cadoni[o,j], F. Calaprice[ae], A. Caminata[l], N. Canci[p], M. Caravati[j], N. Cargioli[o,j], M. Cariello[l], M. Carlini[p,q], M. Carpinelli[ar,aj], S. Catalanotti[s,g], V. Cataudella[s,g], P. Cavalcante[ap,p], S. Cavuoti[s,g,t], A. Chepurnov[e], C. Cicalò[j], A.G. Cocco[g], G. Covone[s,g], D. D'Angelo[ao,v], S. Davini[l], A. De Candia[s,g], S. De Cecco[x,y], G. De Filippis[s,g], G. De Rosa[s,g], A. V. Derbin[z], A. Devoto[o,j], M. D'Incecco[p], C. Dionisi[x,y], F. Dordei[j], M. Downing[ab], D. D'Urso[ar,aj], G. Fiorillo[s,g], D. Franco[ad], F. Gabriele[j], C. Galbiati[ae,p,q], C. Ghiano[p], C. Giganti[w], G. K. Giovanetti[ae], O. Gorchakov[ah,1], A.M. Goretti[p], A. Grobov[aa,ag], M. Gromov[e,ah], M. Guan[ai], Y. Guardincerri[al,1], M. Gulino[1,aj], B. R. Hackett[c], K. Herner[al], B. Hosseini[j], F. Hubaut[f], E. V. Hungerford[a], An. Ianni[ae,p], V. Ippolito[x], K. Keeter[as], C. L. Kendziora[al], I. Kochanek[p], D. Korablev[ah], G. Korga[a,p], A. Kubankin[an], M. Kuss[h], M. La Commara[s,g], M. Lai[o,j], X. Li[ae], M. Lissia[j], G. Longo[s,g], I. N. Machulin[aa,ag], L. P. Mapelli[aq], S. M. Mari[m,n], J. Maricic[af], C. J. Martoff[am], A. Messina[x,y], P. D. Meyers[ae], R. Milincic[af], M. Morrocchi[h,i], V. N. Muratova[z], P. Musico[l], A. Navrer Agasson[w], A.O. Nozdrina[aa,ag], A. Oleinik[an], F. Ortica[at,au], L. Pagani[ac], M. Pallavicini[k,l], L. Pandola[aj], E. Pantic[ac], E. Paoloni[h,i], K. Pelczar[p,u], N. Pelliccia[at,au], E. Picciau[o,j], A. Pocar[ab], S. Pordes[al], S. S. Poudel[a], P. Pralavorio[f], F. Ragusa[ao,v], M. Razeti[j], A. Razeto[p], A. L. Renshaw[a], M. Rescigno[x], J. Rode[p,w], A. Romani[at,au], D. Sablone[ae,p], O. Samoylov[ah], W. Sands[ae], S. Sanfilippo[n,m], C. Savarese[q,p,ae], B. Schlitzer[ac], D. A. Semenov[z], A. Shchagin[an], A. Sheshukov[ah], M. D. Skorokhvatov[aa,ag], O. Smirnov[ah], A. Sotnikov[ah], S. Stracka[h], Y. Suvorov[s,g,aa], R. Tartaglia[p], G. Testera[l], A. Tonazzo[ad], E. V. Unzhakov[z], A. Vishneva[ah], R. B. Vogelaar[ap], M. Wada[ae,j,ak], H. Wang[aq], Y. Wang[aq,ai], S. Westerdale[ae,j], Ma. M. Wojcik[u], X. Xiao[aq], C. Yang[ai], G. Zuzel[u]

[a] *Department of Physics, University of Houston, Houston, TX 77204, USA*
[b] *Instituto de Física, Universidade de São Paulo, São Paulo 05508-090, Brazil*
[c] *Pacific Northwest National Laboratory, Richland, WA 99352, USA*
[d] *Physics Department, Augustana University, Sioux Falls, SD 57197, USA*
[e] *Skobeltsyn Institute of Nuclear Physics, Lomonosov Moscow State University, Moscow 119234, Russia*
[f] *Centre de Physique des Particules de Marseille, Aix Marseille Univ, CNRS/IN2P3, CPPM, Marseille, France*
[g] *INFN Napoli, Napoli 80126, Italy*
[h] *INFN Pisa, Pisa 56127, Italy*
[i] *Physics Department, Università degli Studi di Pisa, Pisa 56127, Italy*
[j] *INFN Cagliari, Cagliari 09042, Italy*
[k] *Physics Department, Università degli Studi di Genova, Genova 16146, Italy*
[l] *INFN Genova, Genova 16146, Italy*
[m] *INFN Roma Tre, Roma 00146, Italy*
[n] *Mathematics and Physics Department, Università degli Studi Roma Tre, Roma 00146, Italy*

[1] Deceased.

[o]Physics Department, Università degli Studi di Cagliari, Cagliari 09042, Italy
[p]INFN Laboratori Nazionali del Gran Sasso, Assergi (AQ) 67100, Italy
[q]Gran Sasso Science Institute, L'Aquila 67100, Italy
[r]Museo della fisica e Centro studi e Ricerche Enrico Fermi, Roma 00184, Italy
[s]Physics Department, Università degli Studi "Federico II" di Napoli, Napoli 80126, Italy
[t]INAF Osservatorio Astronomico di Capodimonte, 80131 Napoli, Italy
[u]M. Smoluchowski Institute of Physics, Jagiellonian University, 30-348 Krakow, Poland
[v]INFN Milano, Milano 20133, Italy
[w]LPNHE, CNRS/IN2P3, Sorbonne Université, Université Paris Diderot, Paris 75252, France
[x]INFN Sezione di Roma, Roma 00185, Italy
[y]Physics Department, Sapienza Università di Roma, Roma 00185, Italy
[z]Saint Petersburg Nuclear Physics Institute, Gatchina 188350, Russia
[aa]National Research Centre Kurchatov Institute, Moscow 123182, Russia
[ab]Amherst Center for Fundamental Interactions and Physics Department, University of Massachusetts, Amherst, MA 01003, USA
[ac]Department of Physics, University of California, Davis, CA 95616, USA
[ad]APC, Université de Paris, CNRS, Astroparticule et Cosmologie, Paris F-75013, France
[ae]Physics Department, Princeton University, Princeton, NJ 08544, USA
[af]Department of Physics and Astronomy, University of Hawai'i, Honolulu, HI 96822, USA
[ag]National Research Nuclear University MEPhI, Moscow 115409, Russia
[ah]Joint Institute for Nuclear Research, Dubna 141980, Russia
[ai]Institute of High Energy Physics, Beijing 100049, China
[aj]INFN Laboratori Nazionali del Sud, Catania 95123, Italy
[ak]AstroCeNT, Nicolaus Copernicus Astronomical Center, 00-614 Warsaw, Poland
[al]Fermi National Accelerator Laboratory, Batavia, IL 60510, USA
[am]Physics Department, Temple University, Philadelphia, PA 19122, USA
[an]Radiation Physics Laboratory, Belgorod National Research University, Belgorod 308007, Russia
[ao]Physics Department, Università degli Studi di Milano, Milano 20133, Italy
[ap]Virginia Tech, Blacksburg, VA 24061, USA
[aq]Physics and Astronomy Department, University of California, Los Angeles, CA 90095, USA
[ar]Chemistry and Pharmacy Department, Università degli Studi di Sassari, Sassari 07100, Italy
[as]School of Natural Sciences, Black Hills State University, Spearfish, SD 57799, USA
[at]INFN Perugia, Perugia 06123, Italy
[au]Chemistry, Biology and Biotechnology Department, Università degli Studi di Perugia, Perugia 06123, Italy

Abstract

Finding unequivocal evidence of dark matter interactions in a particle detector is a major goal of research in physics. Liquid argon time projection chambers offer a path to probe Weakly Interacting Massive Particles scattering cross sections on nuclei down to the so-called neutrino floor, in a mass range from a few GeV to hundreds of TeV. Based on the successful operation of the DarkSide-50 detector at LNGS, a new and more sensitive experiment, DarkSide-20k, has been designed and is now under construction. A thorough understanding of the DarkSide-50 detector response and, therefore, of all types of events observed in the detector, is essential for the optimal design of the new experiment. In this article, we report on a specific set of events, namely, standard two-pulse scintillation-ionization signals with a third small amplitude pulse, occurring within the 440μs data acquisition window of standard events. Some of these events are due to the photoionization of the TPC cathode.

We compare our results with those published by collaborations using liquid xenon time projection chambers, which observed a similar phenomenon, and, in particular, with a recent paper by the LUX Collaboration (D.S.Akerib et al. Phys.Rev.D 102, 092004 (2020)) From the measured rate of these events, we estimate for the first time the quantum efficiency of the tetraphenyl butadiene deposited on the DarkSide-50 cathode at wavelengths of around 128 nm, in liquid argon. Also, both experiments observe events likely related to the photoionization of impurities in the liquid. The probability of photoelectron emission per unit length turns out to be an order of magnitude lower DarkSide-50 than in LUX.

Keywords: Dark matter, liquid argon, underground argon

1. Introduction

The search for direct detection of dark matter in the form of Weakly Interacting Massive Particle Dark Matter (WIMP DM) is one of the most active areas of astroparticle physics. The Liquid Argon (LAr) Time Projection Chamber (TPC) technology offers a path to reach sensitivities to WIMP-nucleus scattering cross-sections down to the so-called neutrino floor [1], for both high and low WIMP masses.

Based on the successful operation of the DarkSide-50 (DS-50) detector [2, 3], a larger and more sensitive experiment, DarkSide-20k (DS-20k) [4], is now under construction. A deep understanding of the DS-50 detector response is one of the key inputs for an optimal design of DS-20k. Therefore, beyond studying events related to dark matter searches, it is very important to scrutinize all event types in the detector, since they may provide indications for detector optimization.

A typical interaction in the active volume of the TPC yields a prompt scintillation signal, S1, and one or more clouds of ionization electrons, depending on the single- or multi-scatter nature of the interaction. Inside the DS-50 LAr TPC, ionization electrons drift upwards under a uniform electric field and are extracted into the gas pocket and induce electroluminescence signals, S2. As discussed in [5], S1 and S2 signals have different pulse shapes. The S1 signal rises in few ns and falls as a double exponential, with $\tau_1 = (6 \pm 1)$ ns and $\tau_2 = (1.5 \pm 0.1)$ μs, and an amplitude ratio of the two exponentials of $\sim$ 3 for nuclear recoils and $\sim$ 0.3 for electron recoils [6, 7]. This difference in amplitude ratios leads to a very effective Pulse Shape Discrimination (PSD) between electron and nuclear recoils. The S2 signal has a different pulse shape, i.e. a ~ 1 μs rise-time and a ~ 3 μs fall-time. The detection of both S1 and S2 pulses allows three-dimensional reconstruction of the interaction point and, therefore, background rejection by detection of multiple interactions and volume fiducialization. In DS-50 the typical pulse charge ratio, S2 over S1, as discussed in section 2, is between 10 and 30. Therefore, low energy interactions may yield only S2 signals above the detection threshold. These single-pulse events were used to extend the search for dark matter to lower masses [2].

In addition to S1+S2 and S2 only events, other event types were also observed in the DS-50 detector. In this paper, we discuss *prompt* emission events, namely events with an additional small amplitude S2 pulse, occurring in the same 440 μs data acquisition window as standard events; we refer to these pulses as Single Electron Candidates (SEC). We classify these events into two different categories: *echo events*, discussed in section 4, when the SEC has a definite tem-

poral relationship with the preceding S1 or S2, and *bulk events*, discussed in section 5, when the SEC does not have a definite temporal relationship with the preceding S1 or S2, but is consistent with being due to a single electron. Therefore, both these event types have features that clearly distinguish them from the common multi-scatter photon background interactions, for which the S2 pulses have a wide spectrum of charges.

We also provide an interpretation of the observed event types based on the study detailed in this paper.

Events with single electron signals occurring outside the acquisition window of a previous standard event, i.e. due to *delayed* emission, were also observed in DS-50 [2] and will be discussed and analyzed in an upcoming DS-50 publication.

Similar kinds of events as those discussed in this paper were also observed and studied with liquid-xenon based detectors. The most comprehensive study was performed by the LUX Collaboration [8] and we use it for comparison with our results. Other previous papers reporting similar event types can be found in Refs. [9, 10, 11, 12].

2. The DarkSide-50 detector

The DS-50 LAr TPC is a cylinder,whose active volume has a height of 35.6 cm and a diameter of 35.6 cm at warm, and contains (46.4 ± 0.7) kg of low-radioactivity argon (UAr) extracted from underground [13, 14, 15]. Arrays of 19 3″ photo-multipliers (PMTs) at each end detect the S1 and S2 signals. The PMTs are immersed in liquid argon and view the active volume through fused silica windows. These are coated on both faces with transparent conductive indium tin oxide (ITO) films 15 nm thick. The inner faces of the window define the grounded anode (top) and the HV cathode (bottom) of the TPC, while the outer faces are kept at the average photocathode potential of each 19-PMT array. The cylindrical side wall is made of 2.54 cm-thick polytetrafluoroethylene (PTFE) reflector that was sintered using a special annealing cycle to increase its reflectivity. The PTFE reflector and the fused silica windows are coated with a tetraphenyl butadiene (TPB) wavelength shifter, which absorbs the 128 nm LAr scintillation photons and re-emits visible photons with a peak wavelength of 420 nm. The specific thickness of the TPB coating on the windows varies between (230 ± 10) μg/cm^2 at the center and (190 ± 15) μg/cm^2 at the edge of the active volume, corresponding to a few μm thickness. The thickness of the TPB on the cylindrical wall is (165 ± 20) μg/cm^2 at half-height and (224 ± 27) μg/cm^2 at the top and bottom. The electric fields needed for drifting and extracting electrons are formed by the ITO-coated cathode and anode planes, a field cage made of a stack of copper rings behind the PTFE reflector held at graded potentials, and a grid that separates the drift and electron extraction regions. The grid is placed 5 mm below the liquid surface. It is made from hexagonal mesh photo-etched from a 50 μm-thick stainless steel foil and has an optical transparency of 95% at normal incidence.

The data reported in this paper were collected between July 2015 and October 2017, with a TPC drift field of 200 V/cm, an extraction field of 2.8 kV/cm, and an electroluminescence field of 4.2 kV/cm. At this extraction field, the grid is fully transparent to electrons and the efficiency for extracting ionization electrons into the gas layer is estimated to be close to 100% [16, 17]. The electron drift time, $t_{\rm drift} = \Delta t_{\rm S2-S1}$, has a maximum value at $t_{\rm drift}^{\rm max}$=376 μs, corresponding to interactions located right above the cathode. The electron drift speed is (0.93 ± 0.01) mm/μs [18].

A hardware trigger in DS-50 occurs when two or more PMT signals exceed a threshold of 0.6 Photo-Electrons (PE) within a 100 ns window. Waveform data are recorded from all 38 PMTs for 440 μs starting $\sim$ 10 μs before the trigger, which, for this analysis, is the S1 signal. Subsequent triggers are inhibited for 810 μs. Software pulse-finding algorithms are then applied to the digitized data, including the pre-trigger data. The software classifies the pulses into two categories (S1 or S2) based on the fraction of light detected within the first 90 ns (f_{90}). The efficiency of the software pulse-finding algorithm is essentially 100 % for S2 signals larger than 30 PE [19]. The pulse finder uses an integration window of 30 μs, which is long enough to include the entire S2 signal.

The argon is purified continuously by recirculating it in gaseous form through a heated getter (SAES Monotorr PS4-MT50-R-2), which reduces contaminants such as H_2O, O_2, and N_2 to sub-ppb levels, and through a cold charcoal radon trap. The measured electron lifetime was greater than $\sim$8 ms during the whole data collection, corresponding to $\sim$35 ppt O_2-equivalent contamination [20].

3. Event selection

We select three-pulse events, with an S1 followed by two S2, one of which is called a SEC. The S1 pulse provides the event trigger. We classify the selected events into two groups, according to the time sequence of the three pulses: S1-S2-SEC, with the SEC occurring after the S2 pulse, and S1-SEC-S2, with the SEC occurring between S1 and S2.

We require the event trigger to occur at least 400 μs after the end of the inhibit window of the previous trigger, namely at least 1.21 ms after the previous trigger. This removes events which were triggered by an S2, with the corresponding S1 occurring during the inhibit window [13].

The S2 light yield drops by about 60% from the center to the sides of the detector [21]. To avoid efficiency corrections for the pulse finder, we only select SEC pulses with the maximum signal in the top central PMT. Furthermore, to avoid anomalous events, we select events with the maximum S2 signal in one of the 19 top PMTs.

The trigger, as shown in Ref.[2], is fully efficient for pulses above 30 PE, and, since all events studied here are triggered by S1, the trigger inefficiency is completely negligible.

The f_{90} variable is also used to distinguish between electron and nuclear recoils. For electron recoils, its value is clustered around 0.3, while for nuclear recoils, it is around 0.7. In this analysis, only electron recoil events are selected, by requiring $f_{90}<$ 0.5. Moreover, to limit the effects of saturation and pulse overlaps, we require S2<50,000 PE and 100 PE <S1<1500 PE.

In DS-50, the typical S2 to S1 charge ratio for electron recoils is between 10 and 30. To further strengthen the identification of the pulse sequence, the S2 to S1 ratio is required to be larger than 10.

4. Echo events

Figure 1 shows the charge of the SEC pulse vs. the time difference, $\Delta t_{\mathrm{SEC-S2}}$, between the SEC pulse and the preceding S2 for S1-S2-SEC events. We observe three main features in the plot, corresponding to three sets of events, which will be detailed in the following sections.

4.1. S2-echo events

One set of events in figure 1 is clustered around $\Delta t_{\mathrm{SEC-S2}} \sim$ 380 μs, corresponding to the maximum TPC drift time, and SEC charges up to a few hundred PEs. It seems

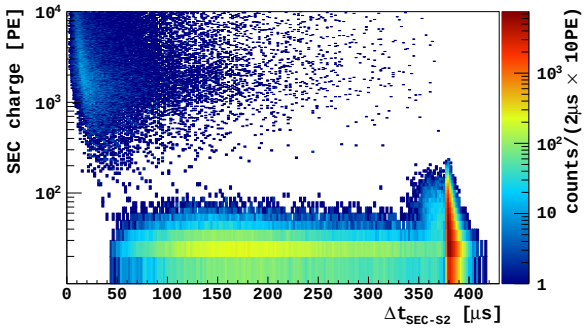

Figure 1: Distribution of SEC charge vs. time difference between the SEC and the preceding S2 pulse, $\Delta t_{\mathrm{SEC-S2}}$.The set of events at small values of $\Delta t_{\mathrm{SEC-S2}}$ and large values of charge is related to double-scatter γ-ray interactions.

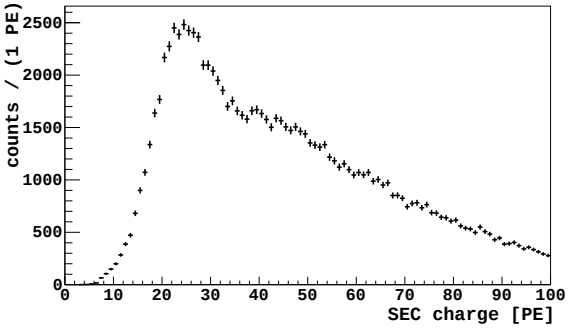

Figure 2: SEC charge distribution for S2-echo events.

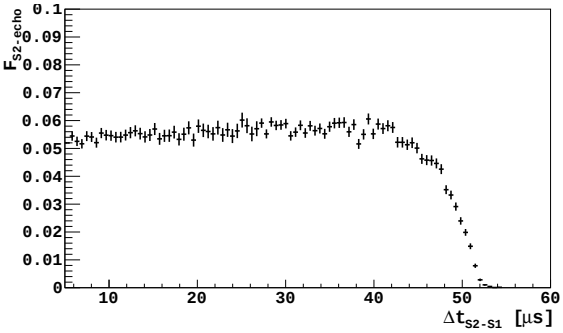

Figure 3: Fraction of events with an S2-echo, as a function of the drift time, $\Delta t_{\mathrm{S2-S1}}$.

plausible that these events are due to S2 photons extracting electrons from the cathode. The electrons then drift through the whole TPC length. We call these events *S2-echo* events. Figure 2 shows the SEC charge spectrum for these events. The peak related to the signal from one ionization electron is clearly visible and its corresponding SEC charge is in agreement with the observation of a previous DS-50 paper [2] of $\sim$ 23 PE. The distribution also shows a tail extending to several electrons. The S2 pulses are quite large signals and can induce the emission of more than one electron from the cathode.

From now on, we require the SEC to be a small amplitude electroluminescence pulse, i.e. to have a charge smaller than 200 PE. This corresponds to about eight extracted electrons. The number of recorded S2-echo events is affected by the data acquisition window of 430 μs after the trigger. This time window is smaller than $2 \times t_{\mathrm{drift}}^{\mathrm{max}}$, the time that would be required for recording all S2-echo events. In practice, the DS-50 data acquisition only records S2-echo events originating from interactions in the top section of the TPC, with drift times, $\Delta t_{\mathrm{S2-S1}}$, smaller than 430 μs$-t_{\mathrm{drift}}^{\mathrm{max}}$, which is $\sim$ 50 μs. Figure 3 shows the fraction of events containing an S2-echo, $F_{\mathrm{S2\text{-}echo}}$, as a function of the drift time, i.e.:

$$F_{\mathrm{S2\text{-}echo}}(t_{\mathrm{drift}}) = N_{\mathrm{S2\text{-}echo}}(t_{\mathrm{drift}})/N_{\mathrm{S2}}(t_{\mathrm{drift}}). \quad (1)$$

The drift time, $\Delta t_{\mathrm{S2-S1}}$, depends on the depth of the interaction, z, with $z = 0$ corresponding to $\Delta t_{\mathrm{S2-S1}} = 0$, the gas-liquid interface.

If our interpretation of the S2-echo events is correct, we should expect that, the larger the S2 charge, the greater the probability of inducing photoelectric emission from the cathode of more than one electron. This indeed is observed in figure 4, which shows the SEC charge vs. S2 charge distribution for S2-echo events. Overlaid is the profile histogram, which clearly shows the expected correlation.

We also expect that the probability of S2-echo events, independent of the SEC pulse charge, increases with the S2 pulse charge.

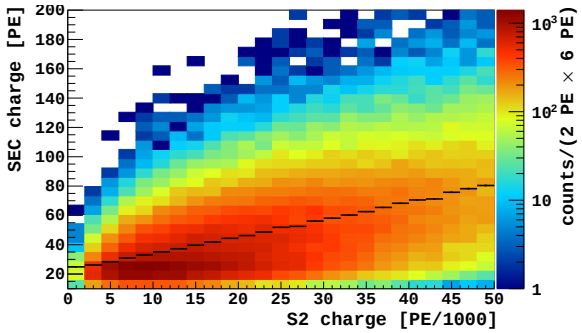

Figure 4: SEC charge vs. S2 charge distribution for S2-echo events. Overlaid is the profile histogram. A linear fit gives an intercept of ∼23.3 PE and a slope of $\sim 1.2 \times 10^{-3}$.

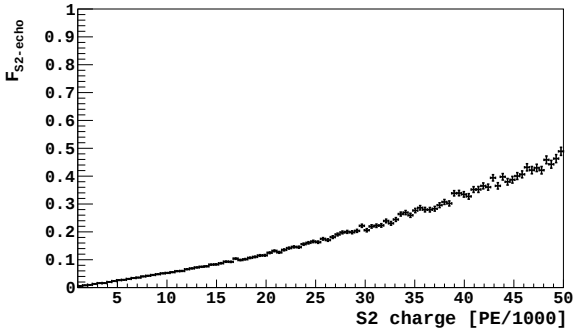

Figure 5: Fraction of S2-echo events vs. S2 charge, with $5\mu s < \Delta t_{S2-S1} < 45\mu s$.

Indeed, this is what is observed in figure 5, which shows the fraction of S2-echo events as a function of the S2 charge. This fraction is found to increase with the S2 charge, leading to an event fraction of about 0.5 at the maximum S2 selected energy. We see that at an S2 of 30,000, the probability of observing an echo as defined is ∼20%. Given our restricted geometric acceptance for the SEC (we only select events with the maximum signal in the central top PMT), this implies that, for events with S2 above this size, essentially every event produced an echo signal in the detector. However, due to the limited data acquisition time window, most of the third pulses are not recorded.

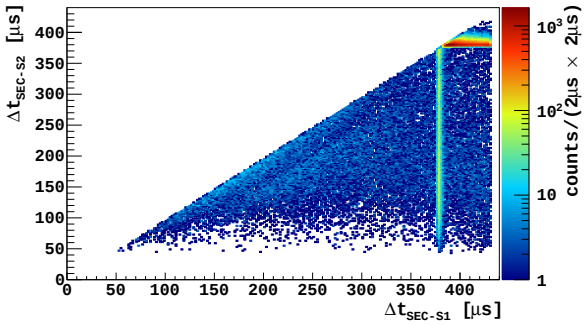

Figure 6: Time difference $\Delta t_{\mathrm{SEC-S2}}$ vs. time difference $\Delta t_{\mathrm{SEC-S1}}$ distribution for events with SEC<50 PE.

4.2. S1-echo events

Another set of events in figure 1 is clustered at SEC charges peaking at ∼25 PE, the single ionization electron response, and spanning the time axis from 50 μs to 375 μs. These events are well separated from those with SEC charges larger than a few 100 PEs, which are identified as S2 events from standard double-scatter γ-ray interactions in the detector. It can be noticed that the pulse finder is not able to reconstruct SEC pulses below ∼ 100 PE that are less than ∼ 40 μs after an S2 pulse.

The origin of these events can be understood from figure 6, which shows the distribution of $\Delta t_{\mathrm{SEC-S2}}$ vs. $\Delta t_{\mathrm{SEC-S1}}$, when selecting events with SEC<50 PE.

Three event categories are clearly visible in the distribution: a horizontal band at $\Delta t_{\mathrm{SEC-S2}} \sim 380$ μs, corresponding to the S2-echo events discussed in section 4.1, a continuum of events without a specific time relation of the SEC with either S1 or S2, which will be discussed in section 5, and a vertical band, corresponding to $\Delta t_{\mathrm{SEC-S1}} \sim 380$ μs, about one maximum drift time after the S1 signal. We interpret these events as photoelectric emissions from the cathode induced by S1 photons and call them *S1-echo* events. Figure 7 shows the time distribution, $\Delta t_{\mathrm{SEC-S1}}$, for events with SEC<50 PE and $\Delta t_{\mathrm{SEC-S2}} < 350$ μs. The narrowness

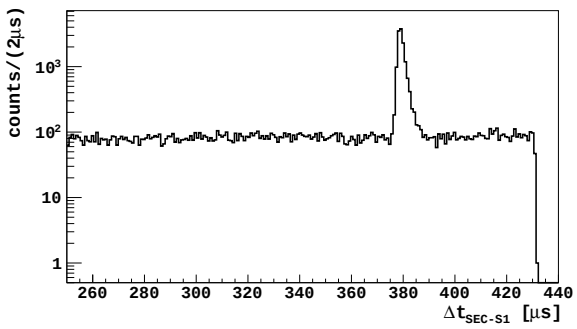

Figure 7: Time difference $\Delta t_{\mathrm{SEC-S1}}$ distribution, for events with SEC<50 PE and $\Delta t_{\mathrm{SEC-S2}} < 350$ μs.

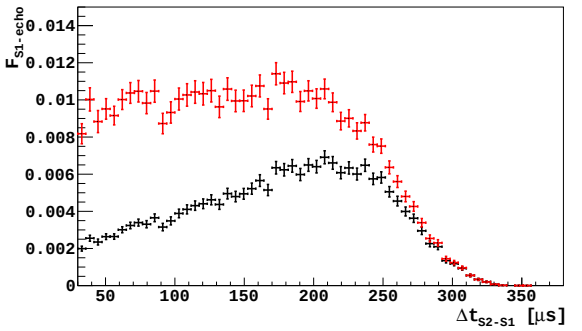

Figure 8: Fraction of S1-echo events, $F_{\mathrm{S1\text{-}echo}}$, vs. drift time $\Delta t_{\mathrm{S2-S1}}$ (black dots) and after S1 UV photon corrections (red dots), $F^{\epsilon}_{\mathrm{S1\text{-}echo}}$. $F^{\epsilon}_{\mathrm{S1\text{-}echo}}$ is multiplied by 0.01 to fit conveniently on the plot.

of the peak for the S1-echo events and the similarity between the rates before and after the peak imply that there is no substantial delayed emission from the liquid surface on the scale of 10 to 100 μs. This finding agrees with the electron extraction efficiency into the gas pocket being close to 100%, as mentioned in section 2. The events before and after the peak belong to the S2-bulk category and are discussed in section 5.

Figure 8 shows the fraction of S1-echo events, $F_{\mathrm{S1\text{-}echo}}$, vs. the drift time, t_{drift}, defined as:

$$F_{\mathrm{S1\text{-}echo}}(t_{\mathrm{drift}}) = \frac{N_{\mathrm{S1\text{-}echo}}(t_{\mathrm{drift}})}{N_{\mathrm{T}}(t_{\mathrm{drift}})}, \qquad (2)$$

with $N_{\mathrm{T}}(t_{\mathrm{drift}})$ the selected total number of events (two pulse and three pulse). The fraction $F_{\mathrm{S1\text{-}echo}}$ rises with t_{drift} up to about 250 μs, due to solid angle effect, whereas it drops at large t_{drift}, when the time of the SEC becomes closer to the preceding S2. This drop is due to a pulse finder inefficiency, similar to the effect seen in figure 1, which tends to merge small signals with a preceding S2. Indeed, when for instance, we select low energy events, such as with S1<800 PE and S2< 5000 PE, we find that the drop at large $\Delta t_{\mathrm{S2-S1}}$ only starts at ~ 300 μs. No tuning of the pulse finder algorithm was made to cope with this effect. We tested the hypothesis that the drop could be due to the SEC being captured by the ion cloud of the S2 signal, by selecting events for which the S2 signal maximum is not in the central PMT. The corresponding distribution in figure 8 does not change, and we therefore discard this hypothesis. The presence of a time gap between the S2 and the subsequent SEC is also visible in the continuum of events at the bottom of figure 6.

The geometric acceptance for S1 UV photons, $\epsilon(r, t_{\mathrm{drift}})$, defined as the fraction of photons, for which we assume 4π emission at a given r and z position in the chamber, that hits a cathode area corresponding to the central PMT, was calculated with a simple Monte Carlo. In the following, we made the simplifying assumption, true to a good approximation, that the event distribution in t_{drift} and r factorizes. Then, the average $\hat{\epsilon}(t_{\mathrm{drift}})$ is obtained by weighting the geometric acceptance $\epsilon(r, t_{\mathrm{drift}})$ by the normalized radial distribution, $f(r)$, of the S2 pulses measured with data, as:

$$\hat{\epsilon}(t_{\mathrm{drift}}) = \sum_{r} \epsilon(r, t_{\mathrm{drift}}) f(r), \qquad (3)$$

For $t_{\mathrm{drift}} < 330$ μs, the calculated efficiency is a rising function of t_{drift} and can be parametrized as:

$$\hat{\epsilon}(t_{\mathrm{drift}}) = 0.0072 \cdot e^{0.0024 \cdot t_{\mathrm{drift}}} - 0.0054, \quad (4)$$

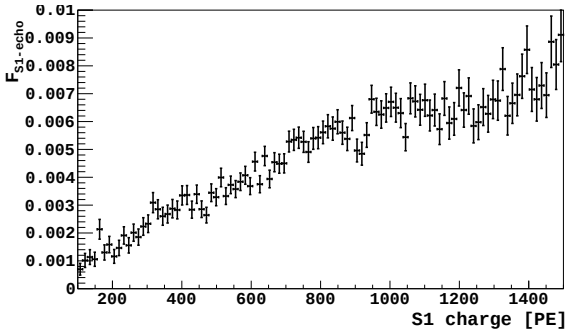

Figure 9: Fraction of S1-echo events vs. S1 charge, with 50 μs $< \Delta t_{\mathrm{S2-S1}} <$ 200 μs.

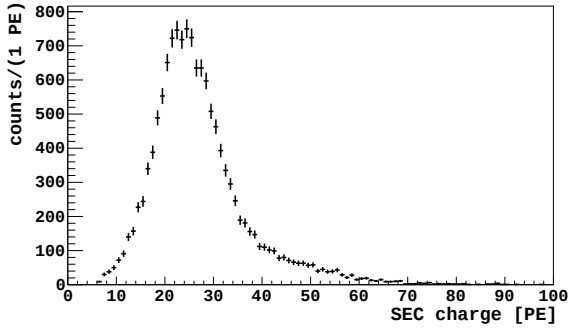

Figure 10: SEC charge distribution for S1-echo events.

with t_{drift} in μs. The fraction of S1-echo events vs. drift time after S1 UV photon acceptance corrections, defined as:

$$F^{\epsilon}_{\mathrm{S1\text{-}echo}}(t_{\mathrm{drift}}) = \frac{N_{\mathrm{S1\text{-}echo}}(t_{\mathrm{drift}})}{\hat{\epsilon}(t_{\mathrm{drift}})N_{\mathrm{T}}(t_{\mathrm{drift}})}, \qquad (5)$$

is shown in red in Figure 8. Below $\sim 200\ \mu s$ we retrieve a flat distribution.

By analogy with figure 5, we show in figure 9 the fraction of S1-echo events vs. S1 charge, with 50 μs $< \Delta t_{\mathrm{S2-S1}} <$ 200 μs. Again, the probability of S1-echo events increases with S1 charge.

Figure 10 shows the SEC charge distribution for selected S1-echo events. The peak corresponding to one extracted electron can be clearly observed. A shoulder due to two extracted electrons can also be noticed.

4.3. Calculation of the cathode quantum efficiency

From the measured fraction of both S1-echo and S2-echo events, it is possible to estimate the quantum efficiency of the cathode in liquid argon, i.e. the photoelectron emission probability per UV photon, γ_{UV}, at the liquid argon emission wavelengths of $\sim$128 nm.

For the calculation of the quantum efficiency measured with S1 photons, QE_{S1}, we select events with 50 μs $< \Delta t_{\mathrm{S2-S1}} <$ 200 μs. Indeed, we have shown in figure 8 that, for these drift times, we retrieve a flat distribution as a function of t_{drift}, after acceptance corrections. The number of S1-echo events is given by:

$$N_{\mathrm{S1\text{-}echo}}(t_{\mathrm{drift}}) = \hat{\epsilon}(t_{\mathrm{drift}})N^{S1}_{\gamma_{UV}}(t_{\mathrm{drift}})\frac{QE_{S1}}{\langle N_{el}\rangle_{S1}}, \qquad (6)$$

where the number of S1 UV photons is given by:

$$N^{S1}_{\gamma_{UV}}(t_{\mathrm{drift}}) = N_{\mathrm{T}}(t_{\mathrm{drift}})\langle S1\rangle_e/g_1. \qquad (7)$$

$N_{\mathrm{T}}(t_{\mathrm{drift}})$ is the selected total number of events (two pulse and three pulse), $\langle S1\rangle_e$ the S1 mean charge expressed in PE, and $g_1 \sim 0.16$ PE/γ_{UV} the average number of photoelectrons per UV photon [21]. The presence of the average number of electrons per S1-echo event, $\langle N_{el}\rangle_{S1}$, in the denominator of eq. (6) takes into account that an S1-echo event might have more than one extracted electron. $\langle N_{el}\rangle_{S1}$ is given by:

$$\langle N_{el}\rangle_{S1} = \langle \mathrm{SEC}\rangle_{\mathrm{S1}}/g, \qquad (8)$$

with $\langle \mathrm{SEC}\rangle_{\mathrm{S1}}$ the average SEC charge of the distribution of figure 10, and $g \sim 23\,\mathrm{PE}/e^-$ the photoelectric gain in the central PMT.

In the selected $\Delta t_{\mathrm{S2-S1}}$ range, the average fraction of S1-echo events, $\langle F^{\epsilon}_{\mathrm{S1\text{-}echo}}\rangle$, is $\sim$ 1.0, see figure 8, and from eq. (5), eq. (6), and eq. (7), we obtain:

$$QE_{\mathrm{S1}} \sim \langle F^{\epsilon}_{\mathrm{S1\text{-}echo}}\rangle \frac{g_1}{\langle S1\rangle_e}\langle N_{el}\rangle_{S1} \qquad (9)$$

The mean value of S1, $\langle S1\rangle_e$, is $\sim$ 730 PE, while the average number of electrons, $\langle N_{el}\rangle_{S1}$, is $\sim$ 1.1, giving a $QE_{\rm S1}$ of $\sim 2.4 \times 10^{-4}/\gamma_{UV}$.

The S2-echo photons are induced by S2 signals, which are all produced within the thin gas region at the top of the TPC. The average acceptance for S2 UV photons, $\hat{\epsilon}_{S2}$, is therefore the value calculated from eq. (4) at $t_{\rm drift} \sim 0$. For S2-echo events, eq. (9) gets modified into:

$$QE_{\rm S2} \sim \frac{\langle F_{\rm S2\text{-}echo}\rangle}{\hat{\epsilon}_{\rm S2}} \frac{g_2}{\langle S2\rangle_e} \langle N_{el}\rangle_{S2} \qquad (10)$$

where the average of $F_{\rm S2-echo}$, $\langle F_{\rm S2\text{-}echo}\rangle \sim 0.055$, is taken from figure 3 over the interval 5 μs $< \Delta t_{\rm S2-S1} <$ 45 μs, $\langle S2\rangle_e$ is the mean S2 charge, $\langle N_{el}\rangle_{S2}$ is the average number of electrons per S2-echo event,

$$\langle N_{el}\rangle_{S2} = \langle {\rm SEC}\rangle_{\rm S2}/g, \qquad (11)$$

with $\langle {\rm SEC}\rangle_{\rm S2}$ the average charge of the distribution of figure 2, yielding $\langle N_{el}\rangle_{S2} \sim 2.1$.

The mean S2 charge, $\langle S2\rangle_e$, is $\sim$ 23,430 PE, $g_2 \sim g_1 \sim 0.16$ PE/γ_{UV} [21, 22], and $\hat{\epsilon}_{\rm S2} \sim 1.8 \times 10^{-3}$, giving a $QE_{\rm S2}$ of $\sim 4.4 \times 10^{-4}/\gamma_{UV}$.

The two measurements of the quantum efficiency, $QE_{\rm S1}$ and $QE_{\rm S2}$, are in broad agreement with each other. They are affected by systematic uncertainties due to the dependence of both g_1 and g_2 on the interaction position in the detector, at most a 10-20% effect, and to the acceptance calculation for S1 and S2 UV photons. Indeed, both $\hat{\epsilon}(t_{\rm drift})$ and $\hat{\epsilon}_{\rm S2}$ were calculated under the simplifying assumption that the SEC signals with the maximum charge in the top center PMT are only those with electrons extracted from the cathode area corresponding to the center PMT. In this way, the efficiency is slightly underestimated, since electrons extracted just outside that area can still give the same kind of signal. A quick evaluation of the uncertainty on the geometric efficiency calculation can be obtained from the fraction of the detector cross-section which is not covered by the PMTs, which amounts to $\sim$15%.Rayleigh scattering was also not included in the acceptance calculation. An upper bound on the size of this effect could be obtained by re-calculating $\hat{\epsilon}(t_{\rm drift})$ and $\hat{\epsilon}_{\rm S2}$ with the inclusion in the Monte Carlo of the Rayleigh scattering probability for the UV-photons, assuming that every scattered photon is lost. In this extreme case, with a scattering length of 90 cm [23], $\hat{\epsilon}_{\rm S2}$ would decrease by $\sim$30%, whereas $\hat{\epsilon}(t_{\rm drift})$ by only $\sim$15%.

In the calculations of the acceptance for S1 and S2 UV photons, we assumed no dependence on the angle of incidence on the cathode of the photoelectric efficiency and that UV light attenuation in liquid argon is negligible.

The measured absorption length of TPB at 128 nm is about 400 nm [24]. Since this thickness is much smaller than the few microns of the TPB on the DS-50 cathode (see section 2), most of the photoelectric effect we observe is due to electron emission from the TPB itself. The QE we measure is therefore the previously unmeasured quantum efficiency of the TPB in liquid argon. It should also be noted that this may be different from the value measured in vacuum since the effective work function of the TPB could be modified by the electron affinity of the liquid argon, as is expected for liquid xenon [8].

5. Bulk events

5.1. Event features

In addition to the S1-echo and S2-echo vertical and horizontal bands, in figure 6 there is also a continuum of events with no specific values of time differences between

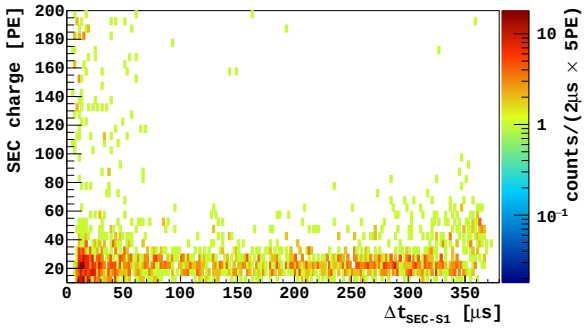

Figure 11: SEC charge vs. time difference $\Delta t_{\mathrm{SEC-S1}}$ distribution, in events with the time sequence S1-SEC-S2.

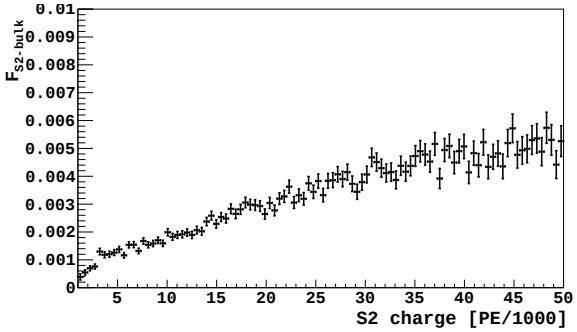

Figure 12: Fraction of S2-bulk events vs. S2 charge, with $\Delta t_{\mathrm{S2-S1}} > 50$ μs.

SEC and either S1 or S2. Since our selection constrains the SEC pulse to follow the S2 one, these events follow the S2 signal, we call them *S2-bulk* events.

It is also possible to observe other events with no specific values of time difference between SEC and S1, by studying events with the time sequence S1-SEC-S2. In figure 11, we show the SEC charge vs. time difference $\Delta t_{\mathrm{SEC-S1}}$ distribution. We notice that these events, apart from the first 30 μs, are evenly distributed in time and with a SEC charge consistent with being single electrons. We call them *S1-bulk* events.

5.2. Interpretation of bulk events

An understanding of the origin of S2-bulk and S1-bulk events is no simple matter. However, at least two observations support that there is a correlation with the S2 and S1 UV photon emission, respectively.

The first observation is that the ratio of the number of observed events (the number of S2-bulk events divided by the number of S1-bulk events) is similar to the ratio of the pulse charge of S2 and S1. The former ratio, as detailed below, is ~ 19, whereas the latter one is ~ 24. To compute the event ratio, we selected the S2-bulk events by requiring 5 μs $< \Delta t_{\mathrm{S2-S1}} <$ 45 μs and the S1-bulk ones by requiring $\Delta t_{\mathrm{S2-S1}} > 354$ μs, i.e. with S2 events at the top of the chamber and the S1 events at the bottom. These time windows were selected with a proper normalization: the corresponding number of total selected events in these windows, two pulse and three pulse events, is the same and they also allow for approximately equal path lengths for the UV photons in the liquid. We also require $\Delta t_{\mathrm{S1-SEC}} > 30$ μs to avoid events which could be related to grid ionization, as discussed at the end of this section. In this way we find 8348 S2-bulk events and 432 S1-bulk events, giving a ratio of ~ 19.

Note that while we ascribe all SEC after S2 as S2 bulk events, in fact for $\Delta t_{\mathrm{SEC-S1}}$ up to the maximum drift time, the source (S1 or S2) is not determined. Given the observed ratio of a SEC formation by S2 or S1, this is a small correction.

The second observation is that the fraction of both S2-bulk and S1-bulk events increases with S2 and S1 charge, respectively, as shown in figure 12 and figure 13.

A candidate explanation for S2-bulk events is the photoionization of contaminants by S2 photons (or S1 photons). One possibility is a contaminant that captured an electron during a previous event, such as, for instance, the O_2^- ion, which has an ionization energy lower than the 9.76 eV energy of VUV argon photons. Photoionization of neutral molecules such as O_2 or H_2O is less likely since the first ionization energy

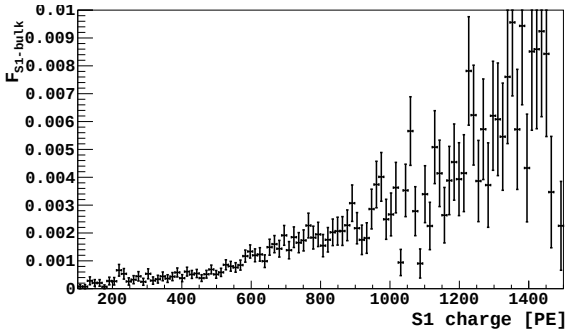

Figure 13: Fraction of S1-bulk events vs. S1 charge, normalized to two-pulse events with 5 μs $< \Delta t_{\mathrm{S2-S1}} <$ 45 μs.

is above 9.76 eV. Another potential contaminant is TPB, which can detach from the walls and dissolve in the liquid [25].

Due to the SEC pulse selection requirement of having the signal maximum in the central PMT, we tend to rule out the interpretation of S2-bulk events as photoelectric emissions from the walls.

We do not favor the possible interpretation of the S2-bulk events as being due to recombination or de-excitation of contaminant molecules since these mechanisms are not expected to yield electrons.

From the fraction of S2-bulk events,

$$F_{\mathrm{S2\text{-}bulk}} = \frac{N_{\mathrm{S2\text{-}bulk}}}{N_{\mathrm{T}}}, \qquad (12)$$

with $N_{\mathrm{S2\text{-}bulk}}$ the number of selected S2-bulk events and N_{T} the total number of selected events (two-pulse and three-pulse), we derive the probability of photoelectric extraction from the liquid per unit length and per UV photon, PEP_{S2}. Averaging over the interval 5 $\mu s < \Delta t_{\mathrm{S2-S1}} <$ 45 μs, we have

$$PEP_{S2} = \frac{1}{\hat{L}_{\mathrm{S2}}} \frac{g_2}{\langle S2 \rangle_b} \langle F_{\mathrm{S2\text{-}bulk}} \rangle, \qquad (13)$$

with $\langle S2 \rangle_b$ the mean S2 charge for selected S2-bulk events. The quantity $\hat{L}_{\mathrm{S2}}$ is the average S2 path length, defined as:

$$\hat{L}_{\mathrm{S2}} = \sum_r L_{\mathrm{S2}}(r) f(r), \qquad (14)$$

where $L_{\mathrm{S2}}(r)$ is the path length of an S2 photon generated at the radial distance r, that falls inside a cylinder of diameter equal to that of the central PMT and height equal to the maximum TPC drift length. Since $\langle F_{\mathrm{S2\text{-}bulk}} \rangle \sim 0.006$, $\hat{L}_{\mathrm{S2}} \sim 1.5$ cm, and $\langle S2 \rangle_b \sim 18,000$ PE, we obtain $PEP_{S2} \sim 4 \times 10^{-6}\ e^-/\gamma_{UV}/\mathrm{m}$.

A higher than average number of events per unit $\Delta t_{\mathrm{SEC-S1}}$, as well as a higher SEC charge, is observed in figure 11, at small values of $\Delta t_{\mathrm{SEC-S1}}$ below 30 μs. A possible interpretation of these events is the photoionization of the extraction grid by S1 signals, as was observed with the LUX detector [8].

5.3. Additional studies

To further test our interpretation of bulk events as photoionization of contaminants, we performed two more studies.

For S2-bulk events, we analyzed a set of data taken during a time period of five days in July 2015, when the getter used in the closed loop to remove contaminants in the liquid argon was turned off for maintenance. Over this period, we expect an increase in contaminants and, if our hypothesis is correct, in bulk photoionization. This is indeed what we observe with the data, but the increase is relatively modest. Indeed, the fraction of S2-bulk events increased by $\sim$35%.

For S1-bulk events, although it is plausible as discussed in section 5.2 that the SEC may originate from the S1 light, there is still the possibility that the SEC is a remnant from a previous event, e.g. an electron captured by some electronegative impurity and then released randomly in the time window between S1 and S2. To test this hypothesis, we looked at a possible time correlation with the previous events. The time difference of S1-bulk events with any previous event in a time window of 10 s (out of which we only

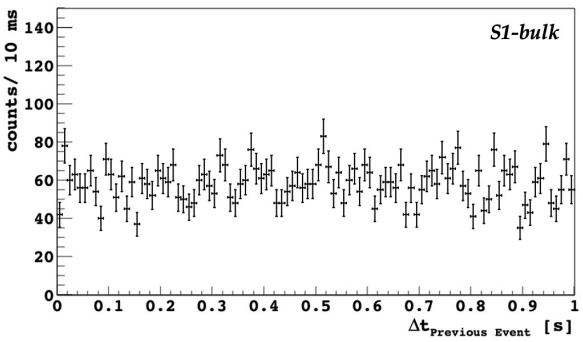

Figure 14: Distribution of the time difference of S1-bulk events with any previous event in a time window of 10 s, for SEC <50 PE. No specific selection cuts to the previous events were applied.

display 1 s), for SEC<50 PE, is shown in figure 14. No specific selection of the previous events is applied, and the time of the events is defined here as the trigger time. According to a simple Monte Carlo simulation that we have performed, a time correlated component would show up as an exponential rise towards zero time. Our data, as shown in figure 14, allow us to exclude a correlated component with $\tau \gtrapprox 20$ ms.

6. Discussion

We observed several categories of single isolated electrons in association with standard scintillation-ionization S1-S2 signals with the DS-50 LAr TPC. Since this is the first study with an argon detector, it is interesting to compare our results to the abundant literature available with xenon detectors. One of the most comprehensive studies was performed by the LUX Collaboration [8] and we mostly compare our results to this one in the following. Section III of that paper reports about four kinds of phenomena: a)*photoionization electrons that are detected within hundreds of microseconds after the S1 and S2 pulses*, b)*delayed emission of individual electrons at the millisecond-to-second scale*, c) *electron emission that appears independent of prior interactions,* and d) *clustered electron emission that occurs within tens of milliseconds after S2.* The present paper gives our experience with the first phenomenon; the second and third are briefly discussed in Ref. [2] and will be treated in more detail in an upcoming DS-50 publication. We do not observe the clustered electron emission that occurs within tens of milliseconds after S2.

6.1. Echo events

S1-echo and S2-echo events are observed both with xenon detectors, namely LUX, ZEPLIN-III [10], XENON100 [11] and with DS-50. The main structural difference between these detectors in this respect is that the DS-50 cathode and anode planes are continuous planes, with the surface facing the active volume coated with ITO and TPB, whereas LUX uses metal grids and there is no wavelength shifting of the light. The quantum efficiency of TPB in DS-50 and that of metal grids in LUX were measured. In both experiments they were calculated with both S1 and S2 photons, and the results agreed in both cases within a factor of two.

In both LUX and DS-50 we observe events that are compatible with photoionization from the extraction grid, right below the gas-liquid interface.

6.2. Bulk events

S1-bulk and S2-bulk events are observed by both LUX and DS-50 Collaborations. Interesting considerations about the origin of S2-bulk events in LUX were obtained from the $\Delta t_{\mathrm{S2-S1}}$ distribution. Unfortunately, due to the limited time window of our data acquisition, we have a severe restriction on the time range of the S2-bulk events, pre-

venting us from making similar considerations.

LUX attributed both S1-bulk and S2-bulk events to the photoionization of impurities dissolved in liquid xenon, more likely neutral molecules than negative ions. The hypothesis of photoionization in the liquid xenon was likewise suggested by the XENON-100 [11] Collaboration, which also showed a correlation of the rate with the electron lifetime, and by the ZEPLIN-II [9] and ZEPLIN-III Collaborations [10].

We observed with DS-50 a correlation with impurity concentration, as the rate of S2-bulk events increased by about 35% during a period of time with the getter switched off. We note that, during the same time period, as described in a previous DS-50 paper [2], we observed a five-fold increase in isolated, i.e., far in time from a standard event, single electrons. Hence, while our data point to an impurity-related origin for photoionozation events, our understanding remains incomplete and inconclusive.

Both LUX and DS-50 measured the probability of photoelectric emission per unit length in the bulk. LUX measured (5-20)$\times 10^{-5} e^{-}/\gamma_{UV}$/m while DS-50 with S2-bulk events measured $\sim 4\times 10^{-6} e^{-}/\gamma_{UV}$/m, i.e., smaller by more than a factor of 10.

While there is no a priori reason the LUX and the DS-50 values for photoelectric emission should be the same, it may be of interest to identify the factors that contribute to the difference in values observed. The measured electron lifetime in DS-50 is much larger than both the lifetime measured by LUX (by more than a factor of 10) and the DS-50 maximum drift time (by a factor of 30). Since the electron attachment rate at the drift field of 200 V/cm (the same for DS-50 and LUX) is about the same for argon and xenon for e.g. O_2 [26], it is plausible that the lifetime difference is mostly driven by a lower concentration of contaminants in DS-50 than in LUX. This conclusion is also coherent with the higher expected outgassing load in a liquid xenon system due to the higher temperature. Concerning the photoionization of negative ions, the different affinities and UV emission energies between liquid argon and liquid xenon may also play a role in the measured PEP_{S2} values.

Unfortunately, identification of the impurity molecules was not possible in both experiments and will have to wait for future research.

It should be noted that the report by LUX [8] is a snapshot in time and that xenon-based experiments have to-date achieved much improved lifetimes.

6.3. Outlook

Given that the same wavelength shifter will be deposited on the cathode of DS-20k, the S1-echo and S2-echo events observed with DS-50 are most likely to be present in DS-20k as well. Given that the aspect ratios of the DS-50 and DS-20k TPCs are almost identical, and that the S2 gain is intended to be the same, the number of echo events will scale with the event rate in the detector. In addition to the event rate factor, there will be a factor of five more S2-bulk events due to the longer drift length of DS-20k, assuming the level of contaminants remains the same.

Acknowledgements

The DarkSide Collaboration offers its profound gratitude to the LNGS and its staff for their invaluable technical and logistical support. We also thank the Fermilab Particle Physics, Scientific, and Core Computing Divisions. Construction and operation of the DarkSide-50 detector was supported by the U.S. National Science Foundation (NSF) (Grants No. PHY-0919363, No. PHY-1004072, No. PHY-1004054,

No. PHY-1242585, No. PHY-1314483, No. PHY-1314501, No. PHY-1314507, No. PHY-1352795, No. PHY-1622415, and associated collaborative grants No. PHY-1211308 and No. PHY-1455351), the Italian Istituto Nazionale di Fisica Nucleare, the U.S. Department of Energy (Contracts No. DE-FG02-91ER40671, No. DEAC02-07CH11359, and No. DE-AC05-76RL01830), the Polish NCN (Grant No. UMO-2014/15/B/ST2/02561) and the Foundation for Polish Science (Grant No. Team2016-2/17). We also acknowledge financial support from the French Institut National de Physique Nucléaire et de Physique des Particules (IN2P3) and the UnivEarthS LabEx program (Grants No. ANR-10-LABX-0023 and No. ANR-18-IDEX-0001), from the São Paulo Research Foundation (FAPESP) (Grant No. 2016/09084-0), from the Interdisciplinary Scientific and Educational School of Moscow University "Fundamental and Applied Space Research", and from IRAP AstroCeNT funded by FNP from ERDF. Isotopes used in this research were supplied by the United States Department of Energy Office of Science by the Isotope Program in the Office of Nuclear Physics.

References

[1] J. Billard, E. Figueroa-Feliciano, and L. Strigari, Phys. Rev. D **89**, 023524 (2014).
[2] P. Agnes et al. (The DarkSide Collaboration), Phys. Rev. Lett. **121**, 081307 (2018).
[3] P. Agnes et al. (The DarkSide Collaboration), Phys. Rev. Lett. **121**, 111303 (2018).
[4] C. E. Aalseth et al. (The DarkSide Collaboration), Eur. Phys. J. Plus **133**, 131 (2018).
[5] P. Agnes et al., Nucl. Instrum. Meth. A **904**, 23 (2018).
[6] M. G. Boulay and A. Hime, Astropart. Phys. **25**, 179 (2006).
[7] A. Hitachi et al., Phys. Rev. B **27**, 5279 (1983).
[8] D. S. Akerib et al., Phys. Rev. D **102**, 092004 (2020).
[9] B. Edwards et al., Astropart. Phys. **30**, 54 (2008).
[10] E. Santos et al., JHEP **12**, 115 (2011).
[11] E. Aprile et al., J. Phys. G **41**, 035201 (2014).
[12] D. Akimov et al., Journal of Instrumentation **11**, C03007 (2016).
[13] P. Agnes et al. (The DarkSide Collaboration), Phys. Rev. D **98**, 102006 (2018).
[14] D. Acosta-Kane et al., Nucl. Inst. Meth. A **587**, 46 (2008).
[15] J. Xu et al., Astropart. Phys. **66**, 53 (2015).
[16] A. Bondar et al., Journal of Instrumentation **4**, P09013 (2009).
[17] E. M. Gushchin, A. A. Kruglov, and I. M. Obodovskil, Zh.Eksp.Teor.Fi. **82**, 1485 (1982).
[18] P. Agnes et al., Journal of Instrumentation **12**, P12011 (2017).
[19] P. Agnes et al. (The DarkSide Collaboration), Phys. Lett. B **743**, 456 (2015).
[20] R. Acciarri et al., Journal of Instrumentation **5**, P05003 (2010).
[21] P. Agnes et al., Journal of Instrumentation **12**, P10015 (2017).
[22] P. Agnes et al., Eur. Phys. J. C **81**, 1014 (2021).
[23] M. Babicz et al., Journal of Instrumentation **15**, P09009 (2020).
[24] C. Benson, G. Orebi Gann, and V. Gehman, Eur. Phys. J. C **78**, 329 (2018).
[25] J. Asaadi et al., JINST **14**, P02021 (2019).
[26] G. Bakale, U. Sowada, and W. F. Schmidt, The Journal of Physical Chemistry **80**, 2556 (1976).